Towards bayesian reconstruction and analysis in bioluminescence tomography via Markov Chain Monte Carlo techniques

Basevi, Hector R.; Guggenheim, James A.; Taylor, Shelley; Dehghani, Hamid; Styles, Iain

DOI:
10.1364/BIOMED.2014.BM3A.45

Document Version
Peer reviewed version

Citation for published version (Harvard):
Basevi, HR, Guggenheim, JA, Taylor, S, Dehghani, H & Styles, I 2014, Towards bayesian reconstruction and analysis in bioluminescence tomography via Markov Chain Monte Carlo techniques. in *Proceedings Biomedical Optics 2014.*, BM3A.45, Biomedical Optics Conference Proceedings 1996-2014, Optical Society of America, Miami, Florida United States, Biomedical Optics 2014, Miami, Florida, United Kingdom, 26/04/14. https://doi.org/10.1364/BIOMED.2014.BM3A.45

Towards Bayesian Reconstruction and Analysis in Bioluminescence Tomography via Markov Chain Monte Carlo Techniques

H.R.A. Basevi,[1,2,*] **J.A. Guggenheim,**[1,2,3] **S.L. Taylor,**[1,2] **H. Dehghani,**[1,2] **and I.B. Styles**[2]

[1]*PSIBS Doctoral Training Centre, University of Birmingham, Edgbaston, Birmingham, B15 2TT, United Kingdom*
[2]*School of Computer Science, University of Birmingham, Edgbaston, Birmingham, B15 2TT, United Kingdom*
[3]*Department of Medical Physics and Bioengineering, University College London, Gower Street, London, WC1E 6BT, United Kingdom*
[*]*hrb886@bham.ac.uk*

Abstract: Spectral bioluminescence imaging and prior knowledge of bioluminescence shape were used to accurately localise, and reconstruct two luminescent sources in a phantom mouse via Markov Chain Monte Carlo sampling, and estimate reconstruction reliability.

OCIS codes: (170.3010) Image reconstruction techniques; (170.6280) Spectroscopy, fluorescence and luminescence; (170.6960) Tomography.

1. Introduction

Bioluminescence is utilised to track and quantify tagged cells via bioluminescence imaging (BLI) and tomography (BLT). The former provides measures of surface fluence over the surface of an imaging subject and the latter can provide a quantitative distribution of bioluminescence in three dimensions, which can then be used to estimate cell numbers and locations. BLT images are typically calculated from BLI images and models of the physical propagation of light through tissue.

There are a number of sources of noise and uncertainty that affect the BLT imaging process including the stochastic nature of photon generation, the degree of tissue scattering and absorption, the surface geometry of the subject (which affects the propagation of light both through the tissue, and between the subject surface and the camera), and the camera noise. A spectral BLT and diffuse optical tomography (DOT) imaging system has been developed [1], which measures the optical properties of subject tissue, the surface geometry of the subject, and the surface fluence indirectly through the use of a model of light propagation in free space within the imaging system. It is desirable to integrate information on all the sources of noise and uncertainty into the image reconstruction process because the reconstruction problem is typically ill-conditioned.

Many reconstruction techniques have been investigated to solve the BLT reconstruction problem. Those techniques that incorporate noise typically assume a normal or Poisson distribution for each measurement. It will be assumed in this case that the signal independent and dependent noise can be approximated as normally distributed. A number of techniques include or assume prior knowledge about bioluminescence distributions in addition to this, whether explicitly (Compressive Sensing [2], Bayesian reconstruction [3]) or implicitly (for example, any algorithm using Tikhonov regularisation based on a Bayesian interpretation). A Bayesian representation is an elegant way to incorporate information regarding uncertainty in terms of both noise and prior information. The result is a posterior probability distribution on the bioluminescence image given the experimental measurements and prior knowledge. An image called the Maximum A Posteriori (MAP) image can be extracted from this posterior distribution by finding the image with the maximum posterior value. Reconstruction of the MAP image has previously been investigated by Feng et al. [3].

The posterior distribution contains all the information available and so has utility beyond the MAP image. If the posterior distribution is multi-modal, those modes can be found and their relative probabilities quantified. The distribution expectation is also useful as it is essentially a weighted sum of all the distribution modes and differs from the MAP estimate when the distribution is asymmetric or multi-modal. Perhaps most interestingly, however, it is possible to extract spatially resolved measures of reconstruction reliability. This work explores these additional measures.

2. Construction of the posterior distribution

In this work an existing multi-modal instrument was used to image a XPM-2 Phantom Mouse (Caliper Life Sciences, A PerkinElmer Company, Hopkinton, Massachusetts, United States of America), which contains two internal fibre-

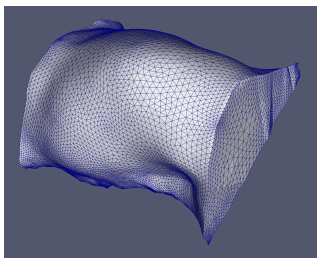

(a) Truncated mouse mesh with the front of the mouse oriented towards the lower right

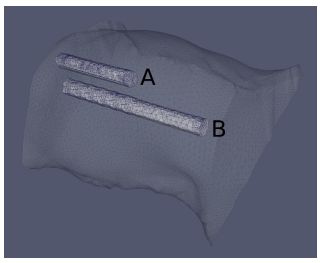

(b) Fibre optic cavities (filled) within mouse mesh with labels

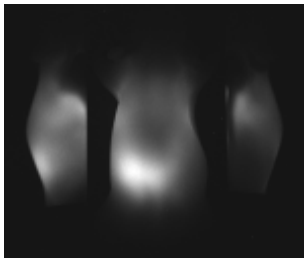

(c) XPM-2 phantom imaged at a wavelength of 640*nm* with both sources switched on

Fig. 1: A truncated mesh of the XPM-2 phantom mouse, acquired using the multi-modal instrument, was used in this work (fig. 1a). The locations of the two tunnels containing the optical fibres are shown in fig. 1b. An image acquired at 640*nm* with both sources switched on is shown in fig. 1c. Three views are available because of the presence of mirrors on either side of the phantom.

fed light sources (fig. 1). A model of the imaging process was formed using the optical properties and geometry of the phantom as measured by the instrument, a model of the free space propagation of light from the phantom to the instrument CCD, and an estimation of the CCD noise properties based on analysis of CCD images acquired without illumination under the assumption of normally-distributed noise. The physical model (fig. 1a) was truncated to remove the head and upper torso, as these regions are so far from the sources that they provide no information. This composite model was used to define a likelihood function.

In the case of the XPM-2 phantom the light sources would ideally be point-like. However the internal structure of the phantom and its light sources is unknown, other than the expected locations of the light sources. Consequently, truncated Gaussian functions were used as a representation, parameterised by a centre location, a width, a maximum intensity, and a threshold distance such that the source strength is zero at any location further from the centre than the threshold distance. A prior distribution was specified based on weak knowledge of the bioluminescent sources:

- No information was provided about the source location.
- The source width was assumed to be associated with a wrapped normal distribution with mean and standard deviation of 5*mm*.
- The source threshold distance was also assumed to be associated with a wrapped normal distribution with mean and standard deviation of 5*mm*.
- The source intensity, which is the number of photons emitted per second at all wavelengths, was assumed to be associated with a wrapped normal distribution with a mean and standard deviation of 8×10^{10} photons per second.
- The distribution was assumed to consist of a single truncated Gaussian function in the case where only one source was switched on, and two truncated Gaussian functions where two sources were switched on.

Measurements were acquired at six wavelengths (560*nm*, 580*nm*, 590*nm*, 600*nm*, 620*nm*, 640*nm*), resulting in tens of thousands of surface measurements for each data set. That number was reduced by combining (by summation) pairs of measurements with an angle between their Jacobian rows of less than 26°. The measurements were then integrated into the likelihood function, and a posterior distribution was formed from the prior and likelihood.

3. Analysis of the posterior distribution

The posterior distribution was examined using Markov Chain Monte Carlo (MCMC) sampling. The Metropolis-Hastings algorithm was used and step sizes were individually optimised for each parameter during a burn-in period. Four independent Markov chains each producing 250 samples were generated and combined for each data set. Estimates of the MAP image, expectation, and standard deviation were calculated from the resulting sample sets.

Reconstruction results can be seen in fig. 2, and are encouraging. The sources are positioned close to the ends of the fibre tunnels, and are similar in size to the tunnel diameters. Further, the two sources possess similar maximum and

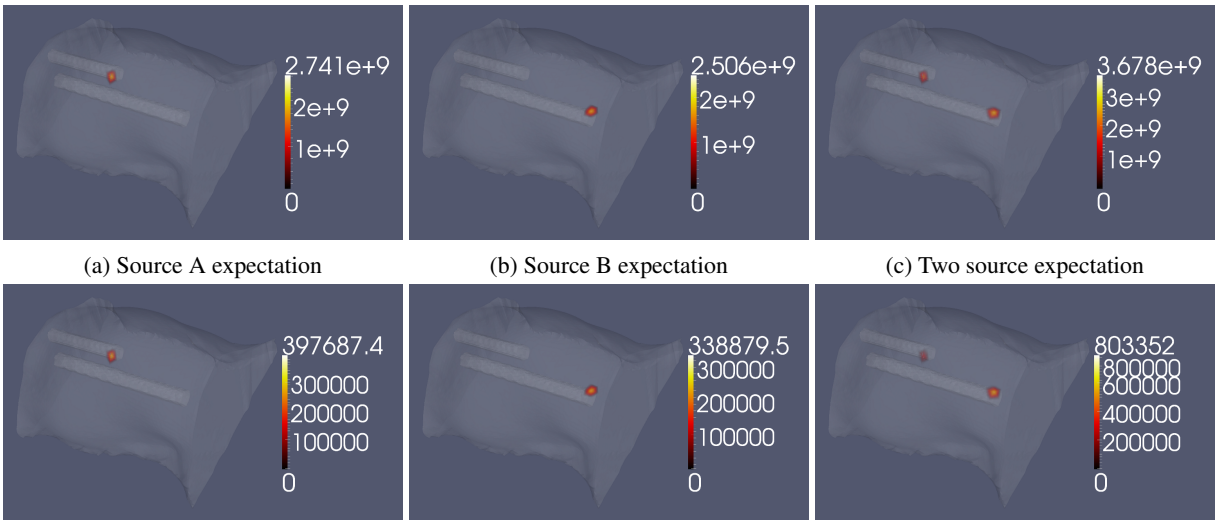

(a) Source A expectation (b) Source B expectation (c) Two source expectation

(d) Source A standard deviation (e) Source B standard deviation (f) Two source standard deviation

Fig. 2: Number of photons emitted per second at all wavelengths, from MCMC sampling of experiments where only source A was switched on (figs. 2a and 2d), only source B was switched on (figs. 2b and 2e), and where both sources were switched on (figs. 2c and 2f). The manufacturer-provided value for the total number of photons emitted per second at all wavelengths within the phantom was $8.09 \times 10^{10} s^{-1}$ for source A and $8.40 \times 10^{10} s^{-1}$ for source B. The reconstructed values were $6.8 \times 10^{9} s^{-1}$ for source A, $8.1 \times 10^{9} s^{-1}$ for source B, and $1.8 \times 10^{10} s^{-1}$ for both sources simultaneously.

total photon production rates, although lower by an order of magnitude than the manufacturer-provided values (fig. 2). The standard deviation plots indicate that the source characteristics are specified to high precision in the posterior distribution, but that this precision suffers when two sources are reconstructed simultaneously, and that this loss of precision predominantly affects the reconstruction of the deeper source.

Reconstruction performance is however dependent on the quality and quantity of experimental measurements. The number of measurements and noise result in a large number of local optima within the posterior distribution, and the large number of measurements result in a large range of posterior distribution values which can make it difficult for the algorithm to leave the locality of a local optimum. This was observed to occur and necessitated the use of multiple independent Markov chains for each data set.

In conclusion, the use of Bayesian techniques and MCMC sampling in BLT shows promise for both reconstruction and reconstruction analysis. The sources were localised accurately and were reconstructed with similar photon production rates. The availability of supplementary information such as a standard deviation map could facilitate interpretation of a reconstructed image. Future work could investigate the use of priors more optimised for particular biomedical applications.

4. Acknowledgments

Funding for this work was provided by EPSRC grant EP/F50053X/1 through studentships to Hector Basevi, James Guggenheim and Shelley Taylor at the PSIBS Doctoral Training Centre at the University of Birmingham.

References

1. J. A. Guggenheim, H. R. A. Basevi, J. Frampton, I. B. Styles, and H. Dehghani, "Multi-modal molecular diffuse optical tomography system for small animal imaging," Meas. Sci. Technol. **24**, 105,405 (2013).
2. H. R. A. Basevi, K. M. Tichauer, F. Leblond, H. Dehghani, J. A. Guggenheim, R. W. Holt, and I. B. Styles, "Compressive sensing based reconstruction in bioluminescence tomography improves image resolution and robustness to noise," Biomed. Opt. Express **3**, 2131–2141 (2012).
3. J. Feng, K. Jia, C. Qin, G. Yan, S. Zhu, X. Zhang, J. Liu, and J. Tian, "Three-dimensional bioluminescence tomography based on bayesian approach," Opt. Express **17**, 16,834–16,848 (2009).